

Chemical Changes in Liquid Benzene Multiply Shock Compressed to 25 GPa

S. Root* and Y. M. Gupta

Institute for Shock Physics and Department of Physics, Washington State University, Pullman, Washington 99164

Received: October 14, 2008; Revised Manuscript Received: December 5, 2008

Shock wave experiments utilizing stepwise-loading, with peak stresses ranging between 4 and 25 GPa, were performed to examine the dynamic high pressure response of liquid benzene at thermodynamic conditions not attainable in single shock experiments. Time-resolved Raman spectroscopy was used to monitor the molecular and chemical changes on sub- μ s time scales. Up to 20 GPa, the Raman modes showed pressure-induced shifting and broadening but no indication of a chemical change. At 24.5 GPa, however, the Raman modes become indistinguishable from an increasing background within 40 ns after the sample attained peak pressure, indicating a chemical change. A thermodynamically consistent equation of state (EOS) was developed to calculate the relevant thermodynamic variables in multiply shock compressed liquid benzene. Idealized molecular configurations were used in combination with the thermodynamic quantities in the shocked state to calculate the intermolecular separation between benzene molecules and to ascertain the likelihood of π -orbital overlap. These idealized calculations show that sufficient energy and π -orbital overlap exist in multiply shock compressed liquid benzene to permit intermolecular bonding at 24.5 GPa. Analysis of the Raman spectra, using the thermodynamic and intermolecular separation calculations, suggests that benzene undergoes polymerization through cycloaddition reactions. The rapid rate of polymerization is attributed to the benzene remaining in a liquid state on the sub- μ s experimental time scale. The results from the present work demonstrate the importance of time, pressure, temperature, and phase in chemical changes associated with π -bonded molecules.

Introduction

Benzene is an important aromatic molecule that serves as a basis for many complex molecules. Several important energetic molecules such as TNT and TATB are built on the benzene ring structure.¹ The delocalized electrons in the π -orbitals of benzene make it extremely stable at ambient conditions, but these π -orbitals are also sensitive to compression. With increasing pressure, π -orbitals of neighboring molecules begin to overlap, resulting in chemical changes through cycloaddition reactions.^{2,3} Thus, a careful examination of the dynamic high-pressure response of liquid benzene is important for understanding not only the benzene response, but also the dynamic high-pressure behavior of more complex π -bonded molecules.

Under static compression, benzene readily freezes into a polycrystalline solid at 0.07 GPa^{4–6} and extensive work on the benzene pressure–temperature phase diagram has been performed.^{7,8} Figure 1 shows the phase diagrams reproduced from refs 7 and 8. Differences in the benzene solid phase region in the two phase diagrams are caused by differences in the time between measurements, whether the sample was annealed, and quality of the benzene crystals formed in the liquid–solid phase transition. A common feature between both phase diagrams is that chemical changes in statically compressed benzene originate from the solid phase. At 4 GPa and 610 °C, benzene undergoes an irreversible chemical change in which the solid benzene forms an amorphous black, carbon substance.⁹ At higher pressures and lower temperatures, solid benzene undergoes an irreversible chemical change into an amorphous C–H polymer

compound.^{7,10–14} However, the chemical changes were not instantaneous and can typically take several hours or more to complete.

Single shock compression experiments by Dick¹⁵ on liquid benzene showed that the benzene Hugoniot had changes in slope at 13.3 and 19.4 GPa. From these results, Dick inferred that benzene undergoes a chemical transformation causing the slope to change starting at 13.3 GPa as opposed to freezing because of the high temperatures generated in these experiments.¹⁵ Yakusheva et al. performed double-pass optical transmission measurements on shock compressed liquid benzene and found that liquid benzene samples became opaque when shocked to a peak pressure of 13.5 GPa.¹⁶ The opacity occurred within 300 ns and was determined to be irreversible. These researchers speculated that their results were consistent with light scattering from carbon particles, indicating decomposition.¹⁶ Holmes et al. also performed double-pass transmission measurements on liquid benzene shocked to peak pressures ranging from 12.4 to 13.8 GPa.¹⁷ In their work, they found that blue light was more attenuated than red light during the experiments. They attributed the transmission loss to Mie-scattering from carbon particles likely formed due to decomposition.¹⁷ However, neither of these studies^{16,17} accounted for the pressure-induced shifting of the π - π^* absorption band, which can cause some of the transmission loss in the blue region.

At pressures above the second slope change in the Hugoniot data (19.4 GPa), Nicol et al. performed emission spectroscopy measurements to determine the products due to shock-induced chemical changes in liquid benzene.¹⁸ The resulting emission spectra showed spectral peaks inferred to be caused by C₂ molecules formed due to benzene decomposition.¹⁸ Experiments that measured the conductivity of shocked liquid benzene above

* To whom correspondence should be addressed. Current address: Sandia National Laboratories, Albuquerque, New Mexico 87185. E-mail: sroot@sandia.gov

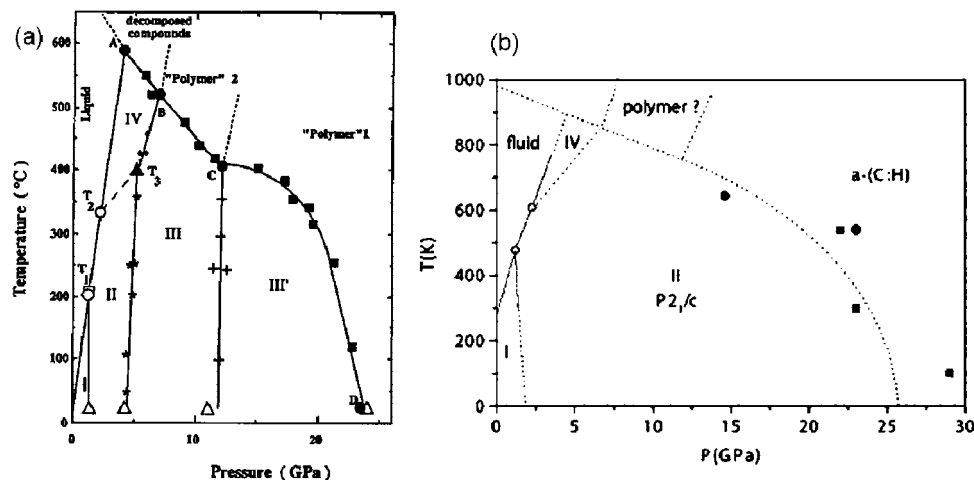


Figure 1. The benzene pressure–temperature phase diagrams: (a) reproduced from ref 7 and (b) reproduced from ref 8.

20 GPa show an increase in conductivity, attributed to an increase in carbon particles.¹⁹ Theoretical work has also suggested that at high shock pressures, carbon clusters (diamond like particles) and molecular hydrogen are likely the dominant decomposition products, but small hydrocarbon molecules may also be present.²⁰

Cyclohexane, a 6-membered nonplanar cyclic hydrocarbon with two hydrogen atoms attached to each carbon and no π -bonding between carbons, did not show a slope change in the Hugoniot data²¹ as was observed in the benzene data. On the basis of differences in the Hugoniot data between benzene and cyclohexane, researchers have proposed that the π -bonds in the benzene molecule influence its shock response at pressures greater than 13 GPa.^{22–25} These hypotheses assume that pressure-induced overlapping of π -orbitals allows for intermolecular bonding to occur through cycloaddition processes, initiating the chemical transformation observed in the benzene Hugoniot. These cycloaddition processes can cause the formation of chemical dimers and have been reported in mass spectroscopy experiments on shock compressed anthracene²⁶ and 2,4,6-TNT.²⁷

The intermolecular bonding mechanisms put forward in refs 22–25 for shocked benzene are similar to the processes described for polymerization in statically compressed solid benzene.¹⁴ However, they are quite different from the decomposition mechanisms suggested in refs 16–20. The final temperatures in singly shocked liquid benzene are typically well above temperatures shown in the phase diagrams in Figure 1. In single shock compression to 13.3 GPa, the calculated temperature, using an equation of state described in a later section, was approximately 1100 °C. At these high temperatures, benzene is known to undergo bond dissociation;²⁸ so comparisons of chemical changes in singly shocked liquid benzene and statically compressed solid benzene are questionable, since the high temperatures likely produce a significant change in the kinetics and the reaction mechanism.

To better understand the phase change kinetics and to be able to better link single-shock and static compression results, benzene samples were compressed to high dynamic pressures in the present work using the multiple shock compression approach.^{29–34} Multiple shock compression results in peak pressure states that are at much lower temperatures than comparable pressure states in single-shock experiments.²⁹ The lower temperatures permit an examination of the phase diagram in pressure–temperature (P – T) regions that are inaccessible in single-shock experiments. In a recent study on multiply shock compressed liquid benzene,³³ we showed that the liquid–solid

phase transition (Figure 1) did not occur on the sub- μ s time scale even though the sample was in a P – T state corresponding to the solid region. Thus, under multiple shock compression, any chemical changes will originate from the liquid state. Recall that due to the high temperatures in single shock compression, the liquid–solid transition is not an issue. Hence, intermolecular interactions in dynamically compressed liquid benzene will differ from those in statically compressed solid benzene because of the lack of an oriented structure under dynamic loading, leading to possible differences in kinetics and reaction mechanisms governing chemical changes.

To examine chemical changes at the molecular level in dynamically compressed liquid benzene, time-resolved Raman spectroscopy measurements were performed in the present study. Time-dependent, pressure–temperature effects on multiply shock compressed liquid benzene were examined to gain insight into the initial stages of the chemical change. A thermodynamically consistent equation of state was developed to calculate changes in pressure, temperature, density, and internal energy.³⁴ From these calculations, the position in P – T space is determined and the changes in the Raman spectra can be correlated to thermodynamic states in the sample.

The objectives of this work, using multiple shock compression, were as follows: (1) to determine the pressure and temperature conditions at which benzene undergoes a chemical change, (2) to determine the time-dependence of the chemical change, and (3) to determine the mechanism of the chemical change. This last objective, specifically, looks to examine whether the chemical change in multiply shocked liquid benzene was consistent with decomposition or polymerization.

Experimental Approach

Figure 2 shows a schematic view of the overall configuration used for time-resolved Raman spectroscopy measurements in our plate impact experiments, and is similar to that used previously in studies on liquid nitromethane.^{30,31} Liquid benzene was obtained from Sigma-Aldrich with a nominal purity of 99.9% and was used without further purification. The benzene samples were confined between two optically transparent windows: z-cut quartz, a-cut sapphire, or LiF $\langle 100 \rangle$ depending on the desired final peak pressure state. The benzene samples were 25.4 mm in diameter and approximately 150–220- μ m thick.

Peak pressure and temperature states ranging from 4.0 GPa and 171 °C to 24.5 GPa and 792 °C were achieved using

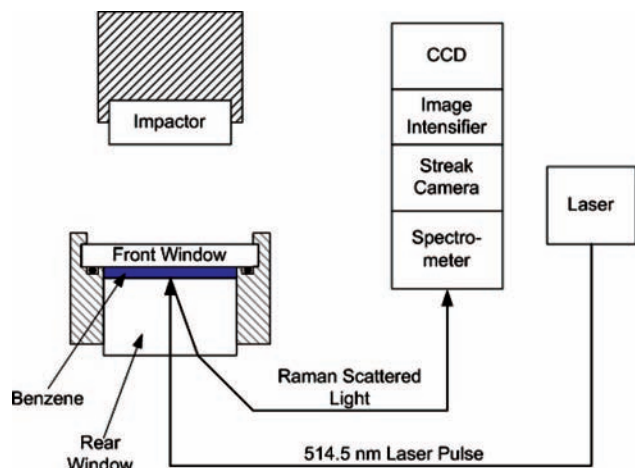


Figure 2. Schematic view of the experimental configuration used for time-resolved Raman spectroscopy measurements.

multiple shock compression.^{29–34} Shock waves were generated by impacting the front optical window with an impactor mounted on a projectile, accelerated to the desired velocities (0.3–2.2 km/s) with a gas gun³⁵ or a powder gun.³⁶ The impactors utilized were z-cut quartz, a-cut sapphire, 6061-T6 aluminum, or OFHC copper depending on the final peak state pressure. Upon impact, a shock wave traveled through the front window and entered the benzene sample. Because of the impedance mismatch between the confining windows and the benzene sample, the shock wave reverberated in the benzene until a uniform peak state was attained. The final pressure in the benzene sample depended only on the shock response of the confining windows and the impactor, and the projectile velocity;²⁹ all of these quantities were well-known for each experiment. Using the reverberation technique, high pressures could be generated in the benzene sample with final peak state temperatures much lower than the temperatures generated in single-shock experiments to the same peak pressure.²⁹

The Raman spectroscopy system was similar to that used in previous work on shock compressed nitromethane.^{30,31} A flash pumped dye laser (Cynosure LFDL-8E), tuned to 514.5 nm (Coumarin dye 504) with a pulse duration of approximately 2 μ s, was used as the Raman excitation source. The laser pulse was delivered to the sample via a 400 μ m diameter optical fiber and approximately 50–60 mJ of energy was focused (1:1 imaging) onto the benzene sample. The scattered light was collected and transmitted via optical fiber to the spectrometer (Kaiser Optics HoloSpec f/1.8i); a 514.5 nm notch filter removed the elastically scattered light. The output of the spectrometer was focused onto a streak camera (Hadland Imacon 790 or Hamamatsu C7700) to temporally disperse the Raman scattered light. The output of the streak camera was amplified using an image intensifier (Phototek, MCP-140) and collected using a CCD (Princeton Instruments), providing intensity–wavelength–time data simultaneously.

The Raman measurements monitored changes in the ν_1 A_{1g} ring-breathing mode (992 cm^{-1}), the ν_2 A_{1g} C–H stretching mode (3061 cm^{-1}), and the ν_7 E_{2g} C–H stretching mode (3043 cm^{-1}). The ν_1 and ν_2 vibrations are the strongest Raman modes in benzene and are easily observed during single-event measurements. At ambient conditions, the ν_7 Raman mode appears as a weak shoulder on the lower frequency side of the ν_2 Raman peak. The Raman data were fit using a Gaussian plus Lorentzian peak function. A polynomial was used to subtract the baseline noise from the data. These three Raman modes provided

information on the C–C and the C–H bonds during the multiple shock experiments, and were used to infer changes in the liquid benzene response.

Equation of State

A thermodynamically consistent equation of state was constructed to calculate the thermo-mechanical response of compressed liquid benzene using theoretical approaches similar to those used for nitromethane³¹ and water.³² A complete equation of state can be constructed from knowledge of the following three thermodynamic quantities: the specific heat at constant volume C_V , the coefficient of thermal pressure $(\partial P/\partial T)_V$, and the isothermal bulk modulus B_T .

For this work, C_V was assumed to be a function of temperature only and was modeled by a single Einstein oscillator function.³⁷ At low temperatures, between the freezing and the boiling point (8 to 77 $^\circ\text{C}$), C_V was fit to known values of the specific heat.^{38–43} At high temperatures (arbitrarily chosen), C_V was fit to the classical value for the specific heat.³⁷

Because liquid benzene freezes at 0.07 GPa at room temperature, extrapolating the liquid benzene isothermal data to high pressures is questionable. Instead, the P – V isotherm was derived from the known Hugoniot data. The Hugoniot data were fitted to 13.3 GPa, the threshold for the chemical change in singly shocked benzene,¹⁵ and then extrapolated as a continuous function to higher pressures. This extrapolation is reasonable because previous work on multiply shock compressed liquid benzene³³ had shown no indications of physical or chemical changes up to 13.3 GPa. The isotherm was related to the fitted Hugoniot using the Mie–Grueneisen equation.⁴⁴ The derivative, $(\partial P/\partial T)_V$ was assumed to be a constant value and was adjusted so that the calculated isotherm matched the known isothermal data at low pressures (<0.07 GPa)⁴³ and the sound speed at ambient conditions.

The complete equation of state was implemented into the COPS wave propagation code,⁴⁵ and used to calculate temperature, density, and energy in the multiple shock compression experiments. The COPS code also provided pressure histories, which were used to determine the time to reach the peak pressure state. The results of these calculations were used in interpreting the Raman measurements.

Experimental Results

Table 1 summarizes the experimental details, in order of increasing peak pressure, for the 15 time-resolved Raman spectroscopy experiments performed in this study. The first column is the experiment identification number. Column 2 shows the measured projectile velocity and column 3 lists the materials utilized as impactors and confining windows. Column 4 lists the benzene sample thickness. The last four columns show the calculated peak state values in the benzene sample. The pressure (P) was calculated from knowing the projectile velocity and the shock response of the impactor and confining windows. The temperature (T), the density (ρ), and the change in internal energy (ΔE) per benzene molecule were calculated using the equation of state implemented into the COPS wave propagation code as described earlier.

Figure 3 shows the measured Raman spectra of liquid benzene at ambient conditions and from three experiments (Table 1) at different peak pressure states. At ambient conditions, the ν_1 ring-breathing mode (992 cm^{-1}) and the ν_2 C–H stretching mode (3061 cm^{-1}) are clearly the strongest modes observed in the benzene Raman spectrum. The ν_7 C–H stretching mode was seen as a shoulder on the low frequency side of the ν_2 C–H

TABLE 1: Summary of Experimental Details

experiment number	projectile velocity (m/s)	expt. configuration impactor/front window/rear window	benzene sample (μm)	P (GPa)	T ($^{\circ}\text{C}$)	calculated peak state values	
						ρ (g/cc)	ΔE (eV/molecule)
TR01 (046) ^a	326	quartz/quartz/sapphire	184	4.1	171	1.38	0.37
TR02 (047) ^{a,b}	1559	Al/LiF/Sapphire	3529	4.2	379	1.36	0.70
TR03 (039) ^a	476	quartz/quartz/quartz	470	4.2	184	1.38	0.39
TR04 (001)	340	sapphire/sapphire/sapphire	187	7.7	197	1.51	0.68
TR05 (041)	353	sapphire/sapphire/sapphire	156	8.0	200	1.52	0.70
TR06 (013)	440	sapphire/sapphire/sapphire	155	10.0	219	1.58	0.88
TR07 (015)	442	sapphire/sapphire/sapphire	145	10.0	219	1.58	0.88
TR08 (043)	1513	Al/LiF/LiF	215	12.6	421	1.63	1.41
TR09 (028)	576	sapphire/sapphire/sapphire	166	13.2	250	1.64	1.16
TR10 (029)	652	sapphire/sapphire/sapphire	163	15.0	270	1.68	1.32
TR11 (042)	1281	Cu/LiF/LiF	166	15.2	495	1.68	1.74
TR12 (036)	873	sapphire/LiF/sapphire	169	16.0	374	1.69	1.59
TR13 (037)	932	sapphire/LiF/sapphire	164	17.3	400	1.71	1.71
TR14 (044)	2171	Al/LiF/LiF	210	19.3	629	1.74	2.32
TR15 (048)	1906	Cu/LiF/LiF	188	24.5	792	1.80	3.05

^a High-resolution Raman measurement. ^b Single-shock experiment

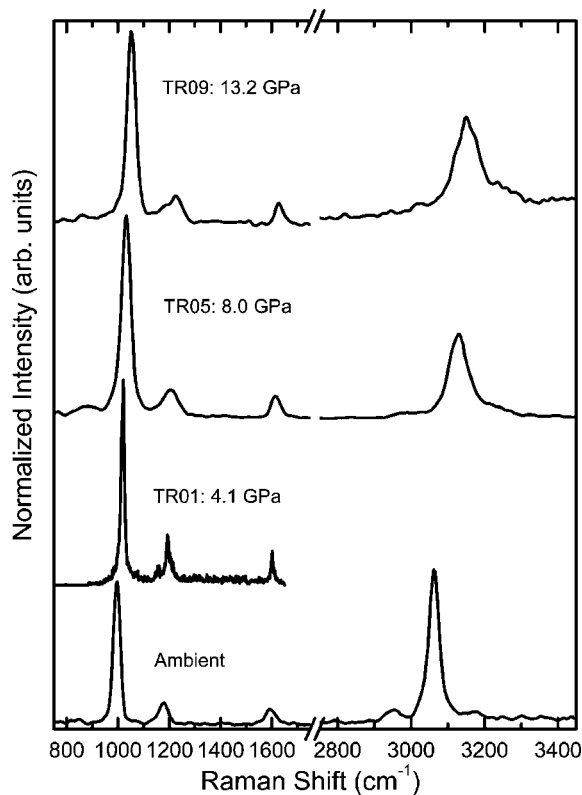


Figure 3. The measured Raman spectra of multiply shock compressed liquid benzene to three different peak pressures. A higher resolution spectral grating was utilized for experiment TR01, which accounts for the narrower peaks and reduced spectral coverage.

stretching mode. Although the ν_9 C–H stretching mode (1178 cm^{-1}) and the ν_8 C–C stretching (1584 cm^{-1}) mode are visible in the spectrum at ambient conditions, their intensities are quite small. Near the $\nu_2 + \nu_7$ C–H stretching modes at 2952 cm^{-1} , the overtone of the IR active ν_{19} E_{1u} C–C stretching vibration was also observed in the ambient spectrum.

As seen in Figure 3, all the Raman modes observed at ambient conditions were also present at the peak pressure states. Even at 13.2 GPa, the onset of chemical changes in singly shocked liquid benzene,¹⁵ all of the Raman modes were observed. This result demonstrates that the high pressure response of liquid

benzene is temperature dependent. At the peak pressure state, the Raman modes were shifted to higher frequency and showed broadening. Once the benzene sample attained peak pressure and the pressure was uniform throughout the sample, the Raman shifts remained nearly constant for the experimental duration. The spectrum at 4.1 GPa (TR01) was measured using a higher spectral resolution grating, reducing the spectral coverage and accounting for the narrower ν_1 Raman peak.

The ν_1 Raman mode in each spectrum showed a similar line shape to the line shape observed at ambient conditions. The $\nu_2 + \nu_7$ C–H stretching mode, however, showed more broadening than the ν_1 ring-breathing mode after the sample attained the peak pressure state. The larger broadening in the C–H modes was likely caused by the ν_2 and the ν_7 modes shifting differently with increasing pressure, as is observed for solid benzene,⁴⁶ and also by the increasing intermolecular interactions due to the increased density and the C–H bond position on the perimeter of the molecule.

Figure 4 shows the time-resolved Raman spectra at five different times from experiment TR13, in which liquid benzene was multiply shocked to a peak pressure of 17.3 GPa and a calculated final temperature of 400 $^{\circ}\text{C}$. At this peak state, the benzene sample was in a P – T state corresponding to the phase diagram region (Figure 1a) near the boundary between solid benzene and a polymerized state.^{7,8} Panel (a) in Figure 4 shows the benzene Raman spectrum at ambient conditions at a time when the shock wave has not yet entered the sample; the dominant ν_1 ring-breathing mode and the $\nu_2 + \nu_7$ C–H stretching modes are clearly visible above the background. Panel (b) shows the benzene Raman spectrum as the sample was loading to peak pressure. At this time, all parts of the sample were not at the same pressure, which accounts for the broadening on the lower frequency side of the Raman peaks. In panels (c)–(e), the benzene sample has attained the peak pressure and temperature state (17.3 GPa, 400 $^{\circ}\text{C}$). All of the main Raman modes were observed for a few hundred ns after the sample attained peak pressure, but the Raman peaks were shifted to higher frequency and showed broadening. Because of the noise inherent in single-event measurements, small fluctuations of the Raman peak shift, width, and intensity exist between the spectra at different times.

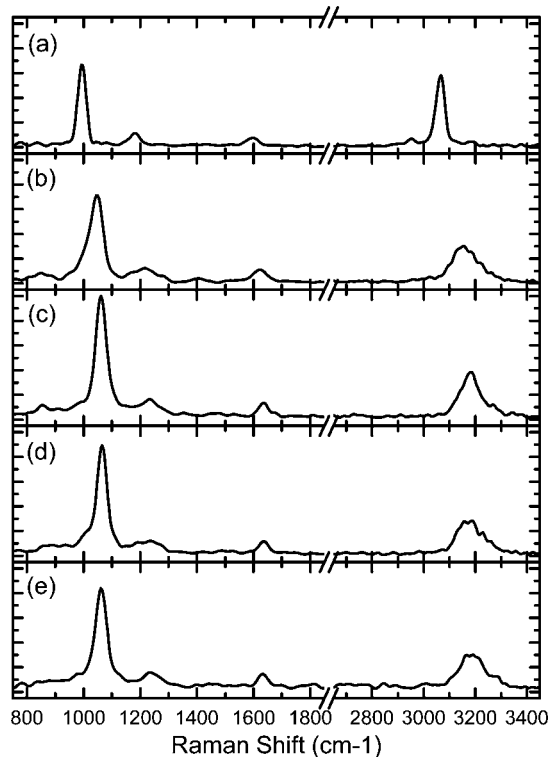


Figure 4. TR13 experimental results: time-resolved Raman spectra of liquid benzene multiply shock compressed to 17.3 GPa. Times relative to the shock entering the sample were (a) -135 ns, (b) 80 ns, (c) 300 ns, (d) 510 ns, and (e) 675 ns. The sample attained the peak pressure state a little after 100 ns.

Panel (e), in Figure 4, shows that the ν_1 ring-breathing mode line shape in the peak state was similar to that observed at ambient conditions. The line shape of the $\nu_2 + \nu_7$ C-H stretching mode, however, showed clear changes in amplitude and width from the ambient spectrum. Changes in the $\nu_2 + \nu_7$ C-H stretching line shape were likely caused by the ν_2 and ν_7 Raman shifts having different pressure dependence, and the broadening of the C-H stretching modes due to increased intermolecular interactions. These line shape changes indicate that the C-H bonds are more affected by changes in pressure (and increases in density) than the C-C bonds in the benzene ring. Although changes in intensity, width, and line shape were observed, the results in Figure 4 indicate that no chemical changes occurred at this pressure-temperature state and on this time scale.

Figure 5 shows the calculated pressure profile for a location in the center of the benzene sample along with the measured Raman shift of the ν_1 ring-breathing mode for experiment TR13 (discussed in Figure 4). The small fluctuations in the Raman shift were caused by noise in the system, unavoidable in single-event measurements at ns time scales. These fluctuations constitute the main uncertainty in fitting the shifted peaks. The error bar shown indicates the standard deviation of the ν_1 Raman shift. Overall, the Raman shifts remained approximately constant after the benzene sample attained the peak pressure state. No temporal changes were observed on this time scale (several hundred ns).

Figure 6 shows the time-resolved Raman spectra from experiment TR14 in which liquid benzene was multiply shocked to a peak pressure of 19.3 GPa and a calculated temperature of 629 °C. The final pressure and temperature state in this experiment was well into the polymer region (Figure 1) of the benzene phase diagrams.^{7,8} At ambient conditions, shown in

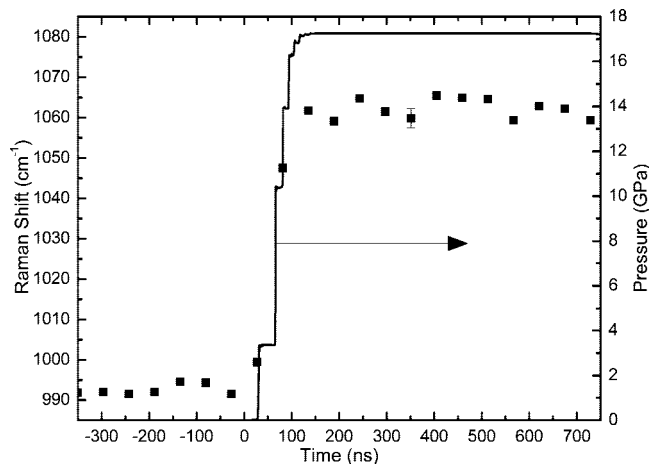


Figure 5. The solid line shows the calculated pressure history at a point in the center of the sample for experiment TR13 using the equation of state developed in this work. Time-resolved measurements of the Raman shift for the ν_1 ring-breathing mode in this experiment have been overlaid. Time is with respect to the shock entering the sample.

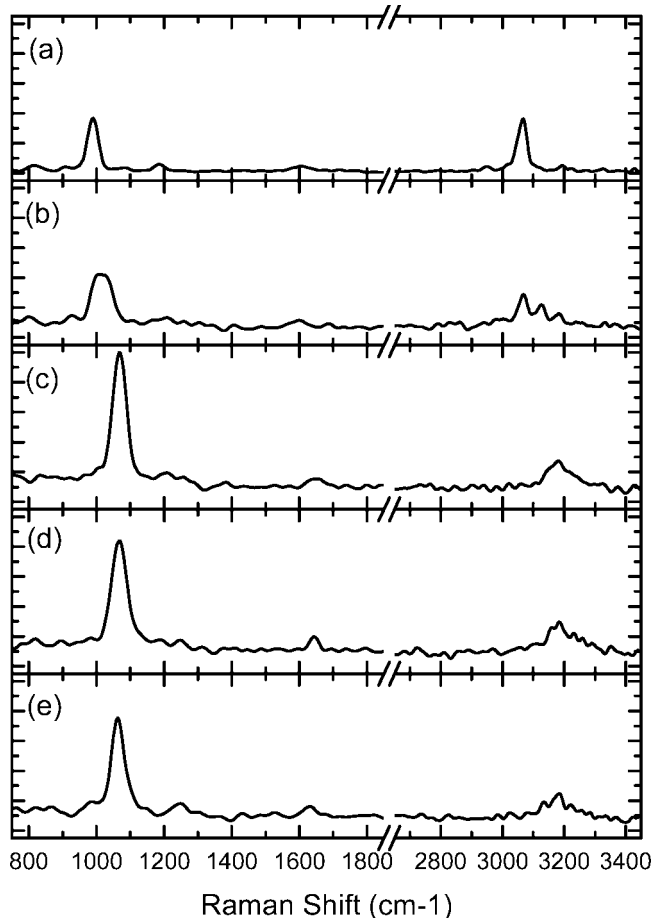


Figure 6. TR14 experimental results: time-resolved Raman spectra of liquid benzene multiply shock compressed to 19.3 GPa. Times relative to the shock entering the sample were (a) -195, (b) 30, (c) 140, (d) 310, and (e) 420 ns. The sample attained the peak pressure state in approximately 80 ns. A possible focusing issue may have occurred in this experiment, which could account for the intensity differences between panel (a) and panels (c,d,e).

panel (a), all the main Raman modes were observed. As the shock entered the sample, the Raman modes begin shifting toward higher frequency as seen in panel (b). The sample has not reached a final, uniform pressure state in panel (b), which

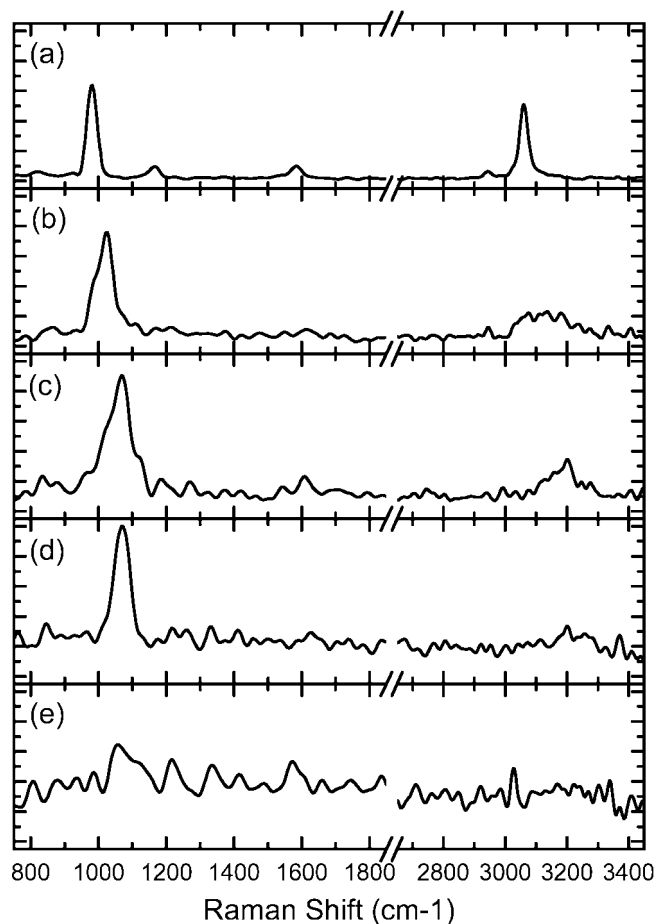


Figure 7. TR15 experimental results: time-resolved Raman spectra of liquid benzene multiply shock compressed to 24.5 GPa. Times relative to the shock entering the sample were (a) -190 , (b) 25 , (c) 60 , (d) 85 , and (e) 105 ns. The sample attained the peak pressure state in approximately 70 ns.

accounts for the broadening observed in the spectrum at this time. Panels (c–e) show the Raman spectra from liquid benzene in the final P – T state. In the peak state, the ν_1 and the $\nu_2 + \nu_7$ Raman modes were still observed above the increased background.

Well after the sample had attained the peak pressure state, the observation of the ν_1 and the $\nu_2 + \nu_7$ Raman modes above the background indicate that no discernible chemical change occurred on the time scale of the experiment. The line shape of the ν_1 mode remained similar to the line shape observed at ambient conditions. However, the $\nu_2 + \nu_7$ C–H stretching modes show significant broadening and amplitude changes. The C–H stretching modes at peak pressure are quite different from the $\nu_2 + \nu_7$ Raman peak observed at ambient conditions and differences can be seen between Figures 4 and 6 at late times, indicating a strong pressure effect on the C–H bonds. Time-dependent intensity changes at late times need to be viewed with some caution. The intensity decrease can occur due to the benzene sample moving out of the focus of the collection lens because of the higher particle velocity generated. This effect was also observed in other lower pressure experiments (TR02, TR08, and TR11 where benzene does not undergo a chemical change) because of the high particle velocities generated in these experiments.

Figure 7 shows the time-resolved Raman spectra from experiment TR15, in which liquid benzene was multiply shocked to 24.5 GPa and a calculated final temperature of 792 °C. Panel

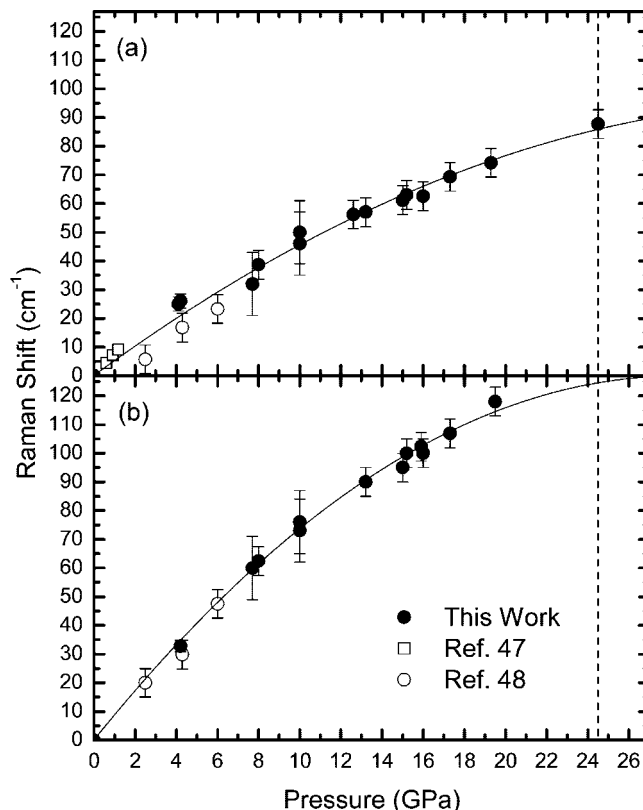


Figure 8. Pressure-induced shifts for (a) the ν_1 ring-breathing mode initially at 992 cm^{-1} and (b) the ν_2 C–H stretching mode initially at 3061 cm^{-1} . The vertical dashed line indicates the peak pressure at which the chemical change was observed. The previous Raman measurements (refs 47 and 48) were limited to 6 GPa. The solid line is a quadratic fit to the data from the present study.

(a) shows the liquid benzene spectrum at ambient conditions prior to when the shock entered the sample. Panels (b) and (c) show the Raman spectrum of the benzene shocking up to the peak pressure state. In panel (d), the benzene sample has attained the final pressure state. The ν_1 ring-breathing mode was clearly observed above the increased background and the ν_1 line shape remained similar to the line shape at ambient conditions. The $\nu_2 + \nu_7$ C–H stretching modes were significantly broadened, and were barely discernible above the increased background. Panel (e) shows the Raman spectrum approximately 40 ns after attaining the peak pressure state. Both the ν_1 and the $\nu_2 + \nu_7$ Raman modes became indistinguishable from the increasing background for the remainder of the experiment. The time at which the Raman modes became indistinguishable from the background was too short to cause the sample to move out of focus of the collection lens. Thus, the time-dependent changes observed in the Raman spectrum were caused by a chemical change in the benzene. To the best of our knowledge, these are the first such observations; the change in the ν_1 mode is noteworthy.

Analysis and Discussion

In all our experiments, the Raman peaks shifted to higher frequency with increasing pressure. Figure 8 shows the Raman shifts of the ν_1 and ν_2 modes as a function of peak pressure up to 25 GPa along with previously published, low pressure data from singly shocked liquid benzene in refs 47 and 48. Our Raman data were best fit with quadratic functions (Figure 8) and the overall Raman data show a monotonic increase with increasing peak pressure. The vertical dashed line indicates the

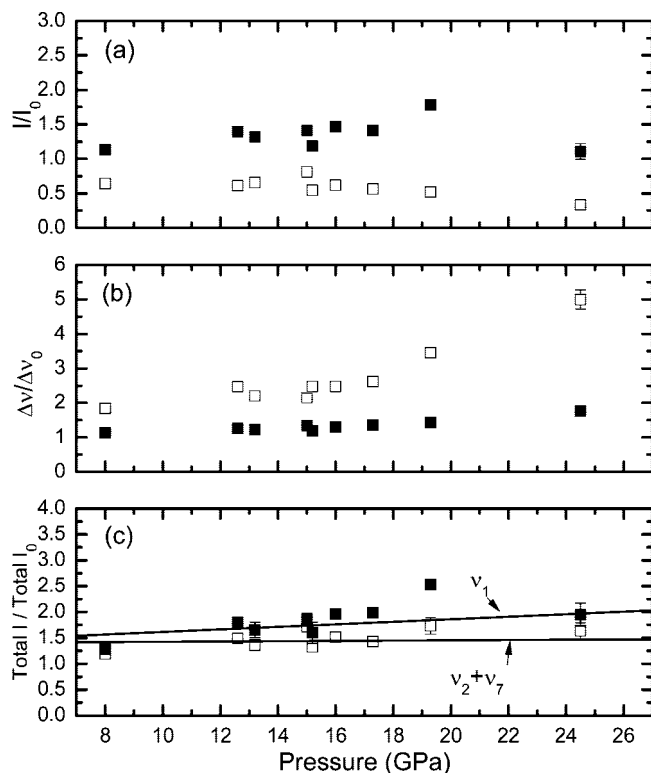


Figure 9. The average shocked-to-ambient ratios for the ν_1 ring-breathing mode and the $\nu_2 + \nu_7$ C–H stretching modes for (a) the amplitude, (b) the full-width at half-maximum (fwhm), and (c) the integrated intensity (area under the Raman peak). The solid line is a linear fit to the data, excluding the point at 19.3 GPa.

peak pressure corresponding to the chemical change indicated at late times in Figure 7. Because of the significant broadening of the C–H stretching modes (Figure 7), a precise measurement of the ν_2 C–H stretching mode shift at 24.5 GPa was not possible. These data demonstrate that the C–H stretching mode shifts more with increasing pressure than the ν_1 ring-breathing mode, indicating that the C–H bonds were more affected by increased pressure (and reduced intermolecular distances) than the C–C bonds in the ring.

While the ν vs P data show a nonlinear response to 20 GPa, no discontinuities were observed in the plot; a strong indication that no liquid–solid phase transition occurred on the time scale of these multiple shock experiments. Previous work³³ had shown no liquid–solid transition to 13 GPa, and a transition was unlikely above 13 GPa due to the higher temperatures generated. As indicated earlier, the chemical changes observed in dynamically compressed benzene originate from the liquid state.

In addition to the frequency shift, the Raman peaks also showed the following changes: the amplitude, the full-width at half-maximum (fwhm), and the total integrated intensity (area under the peak). Figure 9 shows an average of the shocked-to-ambient ratio of these quantities for the ν_1 ring-breathing mode and the $\nu_2 + \nu_7$ C–H stretching modes as a function of peak pressure. For this plot, the ν_2 and ν_7 Raman modes were considered as one peak and the error bars were comparable to the size of the data symbols unless indicated otherwise. Up to 20 GPa, the ν_1 ring-breathing mode was observed to increase in amplitude while the $\nu_2 + \nu_7$ C–H stretching modes decreased in amplitude. Although broadening occurred for both the ν_1 and $\nu_2 + \nu_7$ modes, the increase in the fwhm for the $\nu_2 + \nu_7$ C–H stretching modes was significantly larger than that for the ν_1 ring-breathing mode. The large changes in the fwhm of the C–H

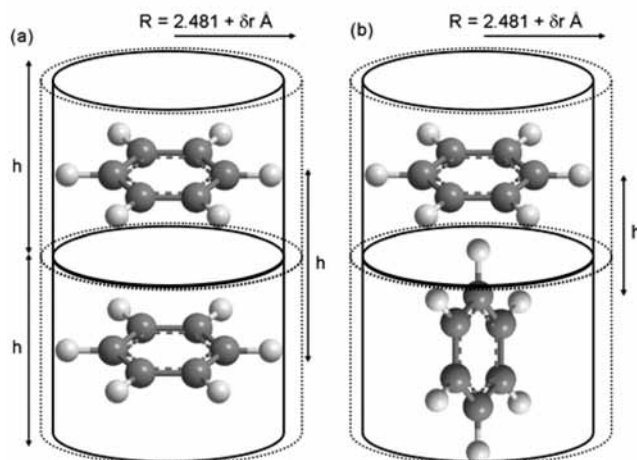



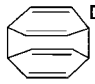
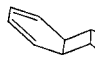
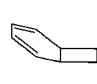
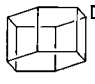
Figure 10. The uniaxial strain, cylindrical model used to estimate intermolecular distances in the multiply shock compressed liquid benzene: (a) stacked configuration with $\theta = 0^\circ$ and (b) T-configuration with $\theta = 90^\circ$.

stretch mode were likely caused by differing pressure dependence of the ν_2 and ν_7 Raman modes, and by broadening due to increased intermolecular interaction. The position of the C–H bond on the benzene molecule makes it more sensitive to density changes. Increased intermolecular interactions may lead to deformations of the dihedral angle of the C–H bonds that can produce a distribution of C–H stretching modes. The increased intermolecular interactions can also cause faster relaxation times, which would further contribute to the broadening of the Raman peaks. The temperature increase in the benzene sample may also account for some of the broadening of the Raman peaks due to vibrational hot bands.⁴⁹

For the ν_1 and $\nu_2 + \nu_7$ Raman modes, the total integrated intensity (approximately, the amplitude times the fwhm) increased as the benzene sample attained peak pressure. Although fluctuations are clearly visible in the shocked-to-ambient ratio data, the integrated intensity ratio never decreased below 1.0 and linear fits (Figure 9c) to the integrated intensity data show small, but slightly positive slopes. The integrated intensity ratio at 19.3 GPa is ignored during the fitting process because of the possible focusing issue. Including this point increases the slope of the linear fit. This finding is a strong indication that no bond dissociation (decomposition) occurred at the P – T conditions of our experiments and for the timescales considered here; bond dissociation would cause the integrated intensity ratio to decrease.

Because our Raman data did not show any bond dissociation, the possibility of polymerization similar to that observed in statically compressed solid benzene needed to be considered. Engelke et al. performed a series of calculations in which two benzene molecules underwent cycloaddition reactions^{23–25} and formed a chemical dimer. Table 2 shows the five chemical dimers, their symmetry, the calculated energy barrier per molecular pair to the formation of the chemical dimer along the concerted pathway, and the calculated reaction distance for the concerted reaction from the work by Engelke et al.^{23–25} The last column in Table 1 lists the change in internal energy (ΔE) per molecule, calculated using the equation of state described earlier, for the multiple shock experiments. A comparison of the two tables shows that in the 19.3 GPa experiment (TR14) enough energy was generated to form the C_5 chemical dimer. However, no chemical change was observed in that measurement indicating that not all of the increase in internal energy

TABLE 2: Benzene Chemical Dimers Predicted by Engelke et al^{23–25}

Engelke Dimers Refs. 23-25	 C _s	 D _{2h}	 C _{2h}	 C _{2v}	 D _{6h}
Energy Barrier (eV/pair)	3.8	5.5	6.7	5.5	11.5
Reaction Distance (Å)	2.1	2.75	2.3	2.1	1.75

can be applied to overcoming the energy barrier to dimerization. When the peak pressure was increased to 24.5 GPa, the increase in internal energy per molecule (when doubled for the dimer) was large enough to overcome the energy barrier to formation for three of the benzene chemical dimers in Table 2. Therefore, intermolecular bonding between benzene molecules is a distinct possibility at 24.5 GPa.

Although sufficient energy was generated to overcome the calculated intermolecular bonding energy barriers, distances between neighboring molecules must also be reduced for significant overlap of the π -orbitals to occur. The reaction distances determined in the calculations by Engelke et al. were on the order of 2.75 Å or less.^{23–25} For statically compressed solid benzene, when lattice vibrations were taken into consideration, Ciabini et al.¹⁴ have recently proposed that intermolecular bonding occurs when intermolecular distances are on the order of 2.6 Å.

Figure 10 shows an idealized uniaxial strain model used to estimate intermolecular distances between molecules in the multiply shocked liquid benzene; the two arrangements shown correspond to two extremes, as discussed below. In this notional approach, the benzene molecules were considered to occupy a cylindrical volume. Because the shock experiment produces uniaxial strain, only the height of the cylinder, h , is changed under shock compression. The radius of the cylindrical volume depends on the C–C and C–H bond lengths, which give a total length of 2.481 Å, and the term δr . The term δr , is reproduced from the work of Ciabini et al.,¹⁴ and provides an estimate of the change in the cylinder radius due to the ν_1 ring-breathing vibration at the different peak pressure and temperature states. The term $\delta r = 3\sigma$, where σ is calculated from

$$\langle \sigma^2 \rangle = \frac{k_B T}{m(2\pi c\nu)^2} \quad (1)$$

k_B is the Boltzmann constant, m = the mass of the carbon atom, T = peak state temperature calculated using the EOS, and ν = the ν_1 ring-breathing mode Raman frequency measured at each peak pressure state. The value of σ was multiplied by 3 to account for the maximum possible variation in the probability distribution.⁵⁰

The molecular volume in the peak pressure state is determined from the peak state density listed in Table 1. At ambient conditions, benzene has a density of 0.8737 g/cm³ that corresponds to a molecular volume of approximately 148.5 Å³/molecule using the benzene molecular weight and Avogadro's number. With the molecular volume and the radius of the cylinder determined, the height of the cylinder, h , is calculated giving an estimate of the intermolecular distances between two parallel stacked molecules (Figure 10a) under uniaxial strain.

Liquid benzene, however, was shown to remain in the liquid state when multiply shocked up to 13 GPa,³³ and at higher pressures and temperatures; no indications of a liquid–solid transition were observed in the Raman data. So a parallel stacked configuration of benzene molecules (Figure 10a) is unlikely to

be present in the shock compressed benzene. To account for the randomly oriented molecules in the liquid, one of the benzene molecules was allowed to rotate through 90° as shown in Figure 10b. The intermolecular separation between neighboring benzene molecules was then calculated as

$$h' = h - (1.397\text{Å} + \delta r)\sin\theta \quad (2)$$

where h is the intermolecular separation calculated for two stacked molecules at a peak state density, 1.397 Å is the radius of the carbon ring of benzene at ambient conditions, δr is the change in radius due to the ν_1 vibration and θ is the angle of rotation between the molecules. $\theta = 0^\circ$ is the parallel stacked configuration (Figure 10a) and $\theta = 90^\circ$ is the T-configuration (Figure 10b). Only the radius of the carbon ring (1.397 Å) is considered in nonparallel stacked configurations since the π -orbitals reside over the carbon ring and not the C–H bonds.

Figure 11 shows the intermolecular separation calculated using the idealized uniaxial strain model discussed above, along with the calculated intermolecular distances (open symbols) for three lattice directions determined from X-ray diffraction data of statically compressed solid benzene at 267 °C, reproduced from ref 14. The black squares show the intermolecular spacing (h) between two parallel stacked benzene molecules (Figure 10a). The black circles show the averaged intermolecular separation, $\langle h' \rangle$, of two benzene molecules in which one molecule was allowed to rotate from 0° to 90° in 5° increments.

Although the intermolecular distances are plotted as a function of pressure in Figure 11, the black squares and circles correspond to different temperatures, as indicated in Table 1. The calculated intermolecular separations show decreasing intermolecular separation with increasing peak pressure, similar to what was observed in statically compressed solid benzene (open symbols). At 24.5 GPa, where the chemical change was observed in the multiple shock experiment, the calculated separation distance for two parallel stacked molecules (Figure 10a) was 3.37 Å, which is approximately 0.77 Å greater than the 2.6 Å threshold proposed by Ciabini et al.¹⁴ When the averaged intermolecular separation $\langle h' \rangle$ at 24.5 GPa is considered the separation distance was approximately 2.41 Å, which is 0.19 Å less than the 2.6 Å threshold. If specific orientations are considered, such as the T-configuration ($\theta = 90^\circ$), shown in Figure 10b, and for $\theta = 45^\circ$, then the intermolecular separation distances are 1.85 and 2.30 Å, respectively. These intermolecular distances are well below the 2.6 Å threshold. Because multiply shock compressed benzene remains in a liquid state, implying a random orientation of the molecules, the intermolecular separations are expected to be less than the 2.6 Å threshold observed for statically compressed solid benzene. Therefore, using an idealized approach, the intermolecular separations in the multiply shocked liquid benzene are reduced to distances suitable for intermolecular bonding as predicted by Engelke et al.^{23–25} and by Ciabini et al.¹⁴

At 24.5 GPa, the intermolecular separation in the liquid benzene has been reduced sufficiently so that significant overlap

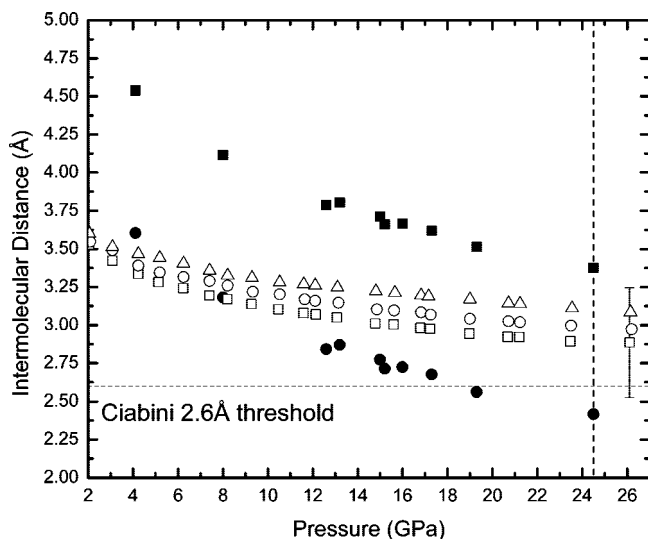


Figure 11. Calculated intermolecular separation distances (between nearest neighbors) in compressed benzene. The open symbols show nearest neighbor distances along different lattice directions calculated from X-ray diffraction data on statically compressed solid benzene (values shown are from ref 14). The filled symbols were determined from the calculated density using the uniaxial strain model shown in Figure 10: ■ intermolecular separation for parallel stacked molecules; ● average intermolecular distance for two benzene molecules in which one molecule is allowed to rotate through 90° in 5° increments. The vertical dotted line indicates the peak pressure at which the chemical change was observed.

of the benzene π -orbitals occurs, comparable to that observed in statically compressed solid benzene and to the theoretical predictions. The calculated internal energy increase was also large enough to overcome the energy barriers to intermolecular bonding. Hence, the chemical change observed in our Raman data is likely due to benzene molecules undergoing cycloaddition processes in which the overlapped π -orbitals of neighboring benzene molecules begin to create σ -bonds like those predicted by Engelke et al.,^{23–25} although these exact dimer formations are unlikely due to the benzene remaining in the liquid state. After the initial chemical dimerization process, the remaining π -electrons in the benzene rings become localized, allowing for further intermolecular bonding to occur readily. We think that the reduced intermolecular separations due to benzene remaining in the liquid state and the higher temperatures likely account for the faster rate of the chemical change in multiply shocked liquid benzene in contrast to statically compressed solid benzene.

Although the formations of these dimers are symmetry forbidden,⁵¹ with the exception of the C_5 dimer,²⁵ the application of high pressure may allow for these processes to occur. The π - π^* transitions are sensitive to pressure and can shift to lower energy with increasing pressure.⁵² This may allow for a thermal transition to an excited-state to occur in the benzene molecules, making these cycloaddition processes symmetry allowed. These pressures and temperatures also likely affect the symmetry of the molecular orbitals, which may create Woodward–Hoffmann symmetry allowed processes.⁵³ However, it is not known how important symmetry considerations are at these pressure/temperature states.

Concluding Remarks

Shock wave compression experiments using stepwise-loading (or multiple shocks) in liquids can access a broad range of thermodynamic states that are not attainable in single shock compression experiments. We have described multiple shock

compression experiments, with peak pressures ranging between 4 and 25 GPa, to examine the high pressure response of liquid benzene at short time scales (sub- μ s) but at P - T conditions that overlap with static compression experiments. Time-resolved Raman spectroscopy measurements were used to monitor the molecular and chemical changes continuously at these short time scales. Up to 20 GPa, the Raman data showed pressure induced shift and broadening of the vibrational modes but no chemical change. At 24.5 GPa, the Raman modes became indistinguishable from an increasing background within 40 ns of the sample attaining peak pressure, indicating a chemical change.

Analysis of the Raman spectra eliminated bond dissociation (decomposition) as the cause of the observed changes in our work. The possibility of polymerization was examined by using a thermodynamically consistent equation of state and idealized molecular configurations in the compressed state to calculate the relevant quantities of interest. These calculations showed that the internal energy and intermolecular separation were sufficient for intermolecular bonding to occur at 24.5 GPa. On the basis of the experimental results and the subsequent analysis presented in the last section, we propose that liquid benzene polymerizes through cycloaddition reactions when multiply shock compressed to 24.5 GPa. The rapid rate of polymerization is attributed to benzene remaining in a liquid state, which increased intermolecular interactions due to reduced intermolecular separation.

The picture that emerges for the high pressure response of liquid benzene at short time scales (sub- μ s) is as follows. Single shock compression, due to high temperatures, causes decomposition. Multiple shock compression results in polymerization, similar to static compression. Rapid polymerization occurs because of the benzene staying in the liquid state at the short time scales in the shock experiments. These results demonstrate that pressure, temperature, time, and even phase play an important role in the high pressure response of benzene, and likely, other π -bonded molecules.

Acknowledgment. The authors thank Drs. A. E. Clark, Z. A. Dreger, and C.S. Yoo for many insightful discussions. Drs. J. N. Johnson and J. M. Winey are thanked for their assistance with the development of the benzene equation of state. Kent Perkins and Kurt Zimmerman are thanked for their technical assistance in performing the shock wave experiments. This work was supported by DOE/NNSA Grant DE-FG03-97SF21388 and the ONR/MURI Grant N00014-01-1-0802.

References and Notes

- (1) Cooper, P. W. *Explosives Engineering*; Wiley-VCH: New York, 1996.
- (2) Drickamer, H. G. *Science* **1967**, *156*, 1183.
- (3) Gilchrist, T. L.; Storr, R. C. *Organic Reactions and Orbital Symmetry*; Cambridge University Press: New York, 1979.
- (4) Bridgman, P. W. *Phys. Rev.* **1914**, *3*, 153.
- (5) Klein, R. M.; Nourbakhsh, M.; Adler, P. N. *J. Mater. Sci.* **1968**, *3*, 657.
- (6) Piermarini, G. J.; Mighell, A. D.; Weir, C. E.; Block, S. *Science* **1969**, *165*, 1250.
- (7) Cansell, F.; Fabre, D.; Petit, J. P. *J. Chem. Phys.* **1993**, *99*, 7300.
- (8) Ciabini, L.; Gorelli, A.; Santoro, M.; Bini, R.; Schettino, V.; Mezouar, M. *Phys. Rev. B* **2005**, *72*, 094108.
- (9) Block, S.; Weir, C. E.; Piermarini, G. J. *Science* **1970**, *169*, 586.
- (10) Pruzan, Ph.; Chervin, J. C.; Thiéry, M. M.; Itié, J. P.; Besson, J. M.; Forgerit, J. P.; Revault, M. *J. Chem. Phys.* **1990**, *92*, 6910.
- (11) Ciabini, L.; Santoro, M.; Bini, R.; Schettino, V. *J. Chem. Phys.* **2002**, *116*, 2928.
- (12) Jackson, B. R.; Trout, C. C.; Badding, J. V. *Chem. Mater.* **2003**, *15*, 1820.
- (13) Santoro, M.; Ciabini, L.; Bini, R.; Schettino, V. *J. Raman Spectrosc.* **2003**, *34*, 557.

- (14) Ciabini, L.; Santoro, M.; Gorelli, F. A.; Bini, R.; Shettino, V.; Raugei, S. *Nat. Mater.* **2007**, *6*, 39.
- (15) Dick, R. D. *J. Chem. Phys.* **1970**, *52*, 6021.
- (16) Yakusheva, O. B.; Yakushev, V. V.; Dremin, A. N. *High Temp.-High Press.* **1971**, *3*, 261.
- (17) Holmes, N. C.; Otani, G.; McCandless, P.; Rice, S. F. In *Proceedings of the Ninth International Symposium on Detonation*; ONCR, Arlington, VA, 1990.
- (18) Nicol, M.; Johnson, M. L.; Holmes, N. C. *Physica* **1986**, *139 & 140B*, 582.
- (19) Nellis, W. J.; Hamilton, D. C.; Mitchel, A. C. *J. Chem. Phys.* **2001**, *115*, 1015.
- (20) Nellis, W. J.; Ree, F. H.; Trainor, R. J.; Mitchell, A. C.; Boslough, M. B. *J. Chem. Phys.* **1984**, *80*, 2789.
- (21) Dick, R. D. *J. Chem. Phys.* **1979**, *71*, 3203.
- (22) Pucci, R.; March, N. H. *J. Chem. Phys.* **1981**, *74*, 1373.
- (23) Engelke, R.; Hay, P. J.; Kleier, D. A.; Wadt, W. R. *J. Chem. Phys.* **1983**, *79*, 4367.
- (24) Engelke, R.; Hay, P. J.; Kleier, D. A.; Wadt, W. R. *J. Am. Chem. Soc.* **1984**, *106*, 5439.
- (25) Engelke, R. *J. Am. Chem. Soc.* **1986**, *108*, 5799.
- (26) Engelke, R.; Blais, N. C. *J. Chem. Phys.* **1994**, *101*, 10961.
- (27) Engelke, R.; Blais, N. C.; Sheffield, S. A.; Sander, R. K. *J. Phys. Chem. A* **2001**, *105*, 6955.
- (28) Smith, R. D.; Johnson, A. L. *Combust. Flame* **1983**, *51*, 1.
- (29) Ogilvie, K. M.; Duvall, G. E. *J. Chem. Phys.* **1983**, *78*, 1077.
- (30) Winey, J. M.; Gupta, Y. M. *J. Phys. Chem. B* **1997**, *101*, 10733.
- (31) Winey, J. M.; Duvall, G. E.; Knudson, M. D.; Gupta, Y. M. *J. Chem. Phys.* **2000**, *113*, 7492.
- (32) Dolan, D. H.; Gupta, Y. M. *Chem. Phys. Lett.* **2003**, *374*, 608.
- (33) Root, S.; Gupta, Y. M. *Chem. Phys. Lett.* **2007**, *442*, 293.
- (34) Root, S. Ph.D. Thesis, Washington State University, WA, 2007.
- (35) Fowles, G. R.; Duvall, G. E.; Asay, J.; Bellamy, P.; Feistmann, F.; Grady, D.; Michaels, T.; Mitchell, R. *Rev. Sci. Instrum.* **1970**, *41*, 984.
- (36) Gupta, Y. M.; Zimmerman, K. A.; Rigg, P. A.; Zaretsky, E. B.; Savage, D. M.; Bellamy, P. M. *Rev. Sci. Instrum.* **1999**, *70*, 4008.
- (37) Callen, H. B. *Thermodynamics and an Introduction to Thermostatistics*, 2nd Ed; John Wiley and Sons: New York, 1985.
- (38) Huffman, H. M.; Parks, G. S.; Daniels, A. C. *J. Am. Chem. Soc.* **1930**, *52*, 1548.
- (39) Burlew, J. S. *J. Am. Chem. Soc.* **1940**, *62*, 696.
- (40) Oliver, G. D.; Eaton, M.; Huffman, H. M. *J. Am. Chem. Soc.* **1948**, *70*, 1502.
- (41) Gorbunova, N. I.; Grigoriev, V. A.; Simonov, V. M.; Shipova, V. A. *Int. J. Thermophys.* **1982**, *3*, 1.
- (42) Burlew, J. S. *J. Am. Chem. Soc.* **1940**, *62*, 690.
- (43) Cibulka, I.; Takagi, T. *J. Chem. Eng. Data* **1999**, *44*, 411.
- (44) Rice, M. H.; McQueen, R. G.; Walsh, J. M. *Solid State Phys.* **1958**, *6*, 1.
- (45) Gupta, Y. M. *COPS Wave Propagation Code*; Stanford Research Institute: Menlo Park, CA, 1976, unpublished.
- (46) Thiéry, M. M.; Léger, J. M. *J. Chem. Phys.* **1988**, *89*, 4255.
- (47) Schmidt, S. C.; Moore, D. S.; Schiferl, D.; Shaner, J. *Phys. Rev. Lett.* **1983**, *50*, 661.
- (48) Kobayashi, T.; Sekine, T. *Phys. Rev. B* **2000**, *62*, 5281.
- (49) Moore, D. S. *J. Phys. Chem. A* **2001**, *105*, 4660.
- (50) Bini, R. private communication.
- (51) Bryce-Smith, D. *Chem. Comm.* **1969**, *14*, 806.
- (52) Drickamer, H. G.; Frank, C. W. *Electronic Transitions and the High Pressure Chemistry and Physics of Solids*; Chapman and Hall: London, 1973.
- (53) Woodward, R. B.; Hoffmann, R. *The Conservation of Orbital Symmetry*; Verlag Chemie GmbH Academic Press Inc.: Germany, 1971.

JP809099W